Active control for multi-degree-of-freedom wave energy converters with load limiting

A.J. Hillis[1], C. Whitlam[2], A. Brask[2], J. Chapman[2], and A.R. Plummer[1]

[1]University of Bath, Department of Mechanical Engineering, Bath BA27AY, UK (e-mail: a.j.hillis@bath.ac.uk, a.r.plummer@bath.ac.uk).

[2]Marine Power Systems Ltd, Ethos Building, Kings Road, Swansea, SA1 8AS (e-mail: contact@marinepowersystems.co.uk).

Abstract

An active control strategy is a key component to enable efficient, safe and economical operation of a wave energy converter (WEC). Many strategies have been developed, but most studies are limited to simplified simulation models of WECs which are not representative of real devices. Furthermore, many studies assume perfect knowledge of the wave excitation force, which is a necessary input to many control strategies. In this work, the aim is to develop an active control strategy to maximise power capture while limiting device loading to prolong its lifetime. An approximate optimal velocity tracking (AVT) controller with a Linear Quadratic Regulator velocity tracking loop is designed. The controller is applied to a validated full-scale nonlinear model of the WaveSub multi-DOF WEC in a range of realistic sea states. Only physically measurable quantities are used in the controller, meaning the strategy developed is deployable in a real system. The performance of the actively controlled system is compared to an optimally tuned passively damped system, and power gains of up to 80% are observed. This approach shows significance in providing a substantial increase in power capture for minimal additional device cost and therefore a major improvement in cost of energy would likely result.

Keywords–Active control, submerged Wave Energy Converter, power take off

I. Introduction

Wave energy still faces many technological challenges on the path to commercialisation, with the over-arching challenge of reducing the cost of energy relative to other renewable sources. Nevertheless the potential resource is recognised as highly significant e.g. [1] and great efforts are being input to pursue the goal of affordable energy production with many new concepts under development. All wave energy converters (WECs) require a power take-off (PTO) to convert the wave input to useful electrical power. The PTO developer faces the challenges of designing systems that can extract energy efficiently from small waves whilst being able to survive high loading in extreme conditions. Many PTO designs are being explored and each has advantages and disadvantages. Classifications of PTO include direct drive electric, hydraulic and mechanical systems. Regardless of the PTO architecture, it must be controllable to maximise efficiency across the wide range of operating conditions it will experience. The control system can also be used to limit load transmission to aid survivability. It is generally accepted that the cost effective WEC and PTO will be highly utilised during the commonly occurring sea states and will shed load in higher sea states, approaching the ideal case termed the "100% sweating WEC" [2]. The control strategy is key to maximising this utilisation, and has its share of challenges.

Active control strategies may be targeted to achieve efficient power capture by keeping the velocity of the primary converter in phase with the wave excitation force. This may be achieved in an ideal manner through complex-conjugate control, for example see [3]. Practical implementation of complex-conjugate control is difficult as it is non-causal and can result in very large forces and motions of the device which could violate physical constraints. Alternative sub-optimal approaches have been proposed, for example latching and declutching control [4][5][6], which engage or disengage the PTO at a specified time. The disadvantage of these strategies is that they can result in large forces being transmitted to the WEC structure and PTO. Model Predictive Control (MPC) strategies have

also been applied, see for example [7][8][9]. These have the advantage that physical constraints can be incorporated, but the optimisation problem may be computationally intensive for a realistic nonlinear WEC and PTO making real-time implementation problematic [10]. Additionally, MPC depends on accurate plant models and requires prediction of the wave excitation force, which increases uncertainty and potentially reduces robustness. More recently pseudo-spectral control has been studied e.g. [11] and purports to have advantages over MPC in terms of computational burden and controlling nonlinear systems. In [12], an experimental study is conducted using an adaptive proportional-integral strategy, which has the advantage of not requiring prediction of the excitation force, but does not incorporate constraints.

Many of these and similar studies are limited to idealised models of single degree-of-freedom (DOF) heaving buoys which are not representative of practical systems. Comparatively little attention has been paid to the control of multi-DOF systems. Abdelkhalik *et al* have studied the control of a 3-DOF floating point absorber which extracts power from heave, surge and pitch motion. They have applied various control strategies including optimal proportional-derivative [13] and pseudo-spectral control schemes [14]. In each case the benefits of large increases in power compared to extracting energy purely in heave have been shown. However, the target device is theoretical only, and no proposition for practical arrangements of PTO systems to achieve the control strategy are provided. Additionally, the system under control is assumed to be modelled precisely which may not be valid. This assumption is common to the majority of WEC control studies conducted in simulation. The Bristol cylinder is one example of a multi-DOF WEC which shares some features with the target device of this study - WaveSub under development by Marine Power Systems Ltd (MPS). It is a submerged tethered cylinder able to extract power from heave, surge and pitch motion [15]. More recently alternative arrangements have been explored [16] with a view to adding practicality to capturing the power. Control of the Bristol cylinder has been considered in [17], though this considers the power electronic hardware rather than active control strategies.

Many active control strategies require knowledge of the wave excitation force acting on the WEC and this is often assumed to be known precisely, even if forward prediction by several seconds is required (e.g. for MPC). These conditions are not realistic for an operational WEC and inevitably real-world performance will be degraded. A control strategy must be robust to modelling errors and other uncertainty, but also must be simple to implement for practical deployment. A suitable candidate solution is the approximate optimal velocity tracking (AVT) controller proposed in [18], whereby a computed velocity reference signal is designed to keep the WEC velocity in phase with the wave excitation while also considering physical constraints such as position limits. Velocity tracking is achieved by a feedback control loop and many architectures are suitable for this purpose. In [19] this strategy is applied to a submerged multi-DOF WEC with three taut tethers using an Internal Model Control loop for velocity tracking. In [20] an adaptive strategy is applied to a 1-DOF WEC to improve performance with a highly nonlinear hydraulic PTO. Here the AVT strategy is applied to a multi-DOF point absorber. A specific WEC (WaveSub) is used to provide a meaningful study and is simulated in the WEC-Sim environment [21]. A Linear Quadratic Regulator state feedback loop is designed for velocity tracking, including full modal coupling. Performance is compared to an optimally tuned passively controlled system in a wide range of irregular sea states.

The motivation for this work is to develop a feasible control system which is applicable to the particular characteristics of the WaveSub WEC and similar devices. This study is distinct from others for the following reasons:

- The target WEC is not purely theoretical and idealised. A validated kinematic nonlinear model is utilised. Experimental systems up to 1:4 scale have been tested and a full scale system is under development.
- The control system is designed around a linearised model of the WEC, but is then tested with the full nonlinear model so modelling errors are inherent and indeed identified.
- The WEC is free to move in all six DOF, though is largely constrained to heave, surge and pitch as it is aligned with planar waves.
- Precise knowledge of the wave excitation force is not assumed. It is estimated from the modelled system dynamics using measurable quantities in a deployable system.
- The performance of the active control system is compared against a well-tuned passive system, so performance gains are not exaggerated.

Thus, the main contribution if this paper is to design and test a deployable control system with a realistic multi-DOF nonlinear WEC in realistic operating conditions. The remainder of the paper is arranged as follows. An overview of the WaveSub WEC is provided in section II. Descriptions of the WEC model and its linearised equivalent are provided in sections III and IV. The control strategy is described in section V with a method for wave force estimation given in section VI. Simulation results comparing the passive benchmark system performance against the actively controlled system under realistic conditions are provided in section VII. Conclusions are provided in section VIII.

II. Overview of the WaveSub WEC

WaveSub is under development by Marine Power Systems Ltd. It is a submerged point absorber with a unique multi-tether configuration and variable geometry which can be tuned to the prevailing sea state. A float moves with the waves and reacts against a moored base. The tethers pull on rotational drums which are attached to a PTO. An illustration of a full scale multi-float concept is shown in Figure 1.

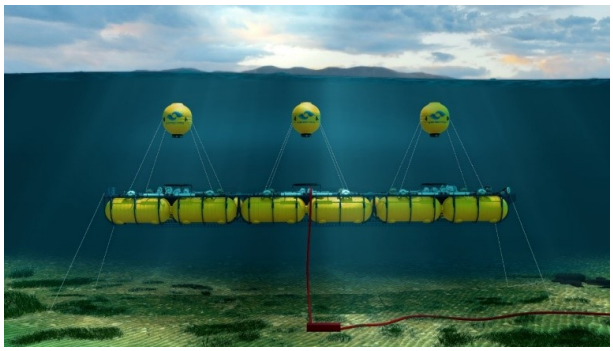

Fig. 1. Illustration of full scale multi-float WaveSub concept

This study uses a single section of this device, comprising a single float with four taut tethers connected to individual drums and rotational PTOs. The block diagram of the complete system is shown in Figure 2.

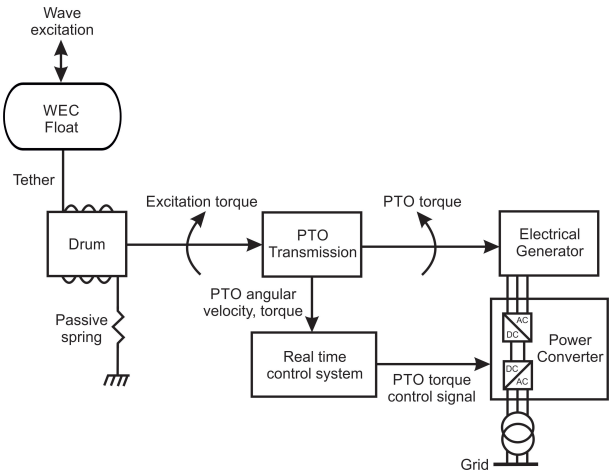

Fig. 2. Block diagram representation of WEC/PTO systems

III. Baseline WEC Simulation

A. Model Description

System models have been created using WEC-Sim [21], an open-source multi-body simulation tool which integrates with Matlab. A 1:25 scale WEC-Sim model of a single float system using four PTO

tethers and a taut mooring system has been validated against experimental data from wave tank testing [22]. A full-scale WEC-Sim model has been extrapolated from the 1:25 scale model and is the subject of this study. The optimum passive spring-damper combinations have been established across the full range of operational irregular sea conditions and this system is used as a benchmark for performance comparison against an actively controlled PTO system. Figure 3 shows an image of the simplified geometry used for simulation in the WEC-Sim package. The dimensions are given in table I.

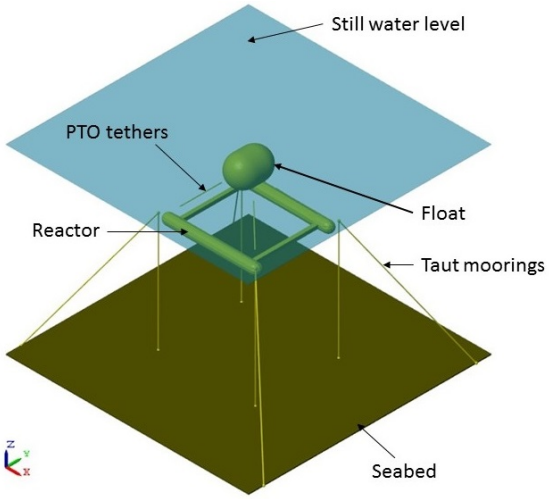

Fig. 3. Simplified geometry and mooring in WEC-Sim

TABLE I
DIMENSIONS OF THE GEOMETRY OF THE FULL SCALE WEC-SIM MODEL

Properties	Value	Unit
Float diameter	12	m
Float cylinder length	4.75	m
Reactor length	51.55	m
Reactor width	50	m
Reactor height	4.85	m

The float and reactor are connected with four taut PTO tether lines, each modelled as a translational PTO actuation force incorporating a spring stiffness and damping force, a universal joint and gimbal. All motions and forces are available for use by the control strategy within this model and the control force applied to each PTO is incorporated by adding to the external preload force on each PTO. The damping force is used only for the benchmark passive optimally tuned system and is set to zero for active control. Irregular waves are applied in the x-direction.

Results using a Pierson-Moskowitz (PM) spectrum with significant wave height $H_s = 3\text{m}$ and energy period $T_e = 10\text{s}$ (see Figure 4) are presented in detail, giving insight into the internal signals and processes occurring within the passive and active control systems. This sea state represents a typical sea state for which the device is sized. A wide range of PM spectra with $H_s = 0.5 - 6.5\text{m}$ and $T_e = 6 - 16\text{s}$ are used latterly for mean power capture comparison. All simulations were for a 700s duration in total with a sample time of 0.02s.

B. Forces acting on the float body

The float body system dynamics are governed by:

$$\mathbf{M}\ddot{\mathbf{x}} = \mathbf{F}_h(t) + \mathbf{F}_m(t) \tag{1}$$

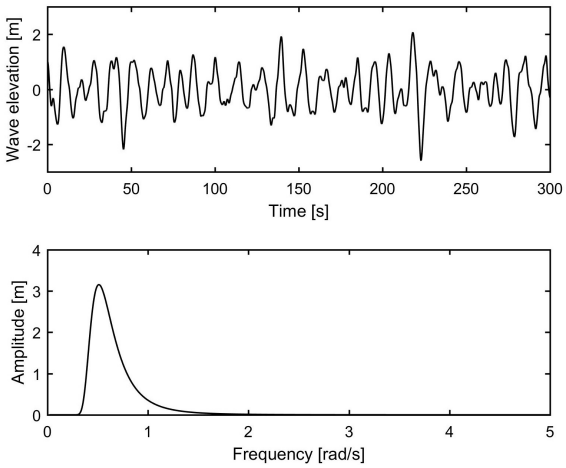

Fig. 4. Wave elevation and spectrum for irregular waves (Pierson-Moskowitz with $H_s = 3\text{m}$ $T_e = 10\text{s}$)

where $\mathbf{M}$ is the float mass matrix, $\ddot{\mathbf{x}}$ is the float acceleration vector, $\mathbf{F}_h(t)$ is the total hydrodynamic force vector and $\mathbf{F}_m(t)$ is the mechanical force vector of the PTO. Assuming linear wave theory, the hydrodynamic force can be decomposed as follows:

$$\mathbf{F}_h(t) = \mathbf{F}_e(t) + \mathbf{F}_r(t) + \mathbf{F}_{hs}(t) + \mathbf{F}_v(t) \tag{2}$$

where $\mathbf{F}_e(t)$, is the excitation force produced by an incident wave on an otherwise fixed body, $\mathbf{F}_r(t)$ is the radiation force which is produced by an oscillating body creating waves on an otherwise still sea, and $\mathbf{F}_{hs}(t)$ is the hydrostatic restoring force. $\mathbf{F}_v(t)$ is a nonlinear viscous damping term which is commonly neglected.

$\mathbf{F}_{hs}(t)$ is constant as the float is fully submerged. In the heave direction it is given by

$$F_{hs}(t) = -\rho g V \tag{3}$$

where ρ is the water density, g is the acceleration due to gravity and V is the float volume.

The radiation force in the time domain is given by [23]

$$\mathbf{F}_r(t) = -\mathbf{A}_\infty \ddot{\mathbf{x}} - \int_0^t \mathbf{K}_r(t-\tau)\dot{\mathbf{x}}(\tau)d\tau \tag{4}$$

where $\mathbf{A}_\infty$ is the infinite frequency added mass matrix, $\mathbf{K}_r$ is the radiation impulse function and $\mathbf{x} \in R^{6\times 1}$ is the state vector given by

$$\mathbf{x} = [x\ y\ z\ \theta_x\ \theta_y\ \theta_z]^T \tag{5}$$

The excitation and radiation forces are calculated using hydrodynamic coefficients computed by the NEMOH boundary element method (BEM) solver [24].

C. Optimal tuning of PTO stiffness and damping

The passively damped system uses a fixed damping coefficient on each PTO, which is dependent on the peak period of the wave spectrum applied. For each sea state tested the passive damping co-efficient and spring stiffness were optimally tuned. The optimal parameters are shown in Figure 5.

As such the passive system benchmark performance represents the highest possible captured power with a fixed damping coefficient in a given sea state. In practice, to achieve this, the damping coefficient would need to vary as the incident sea state changes. This could be achieved using a slow-tuning control strategy (e.g. [25]), but performance will degrade sharply if the damping is poorly tuned. Tuning in operation would depend upon good estimation of the peak energy period of the incident sea-state. This is not always possible due to long data lengths required, and the lack of a defined peak or double peaks in some seas.

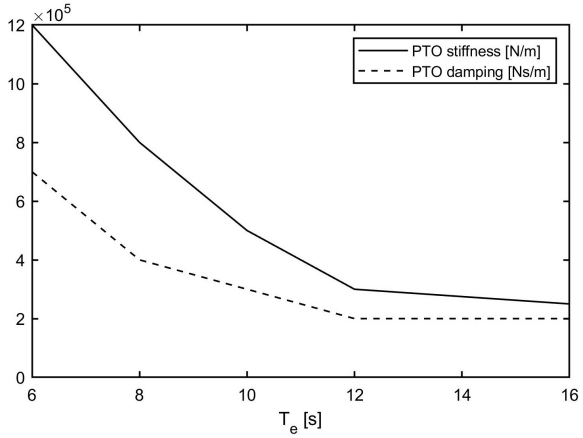

Fig. 5. Optimal stiffness and damping curves for passive WEC

IV. Linearised dynamic system model

A linearised approximation to the WEC and PTO systems is typically required for model-based control system design. Assuming the reactor to be fixed for simplicity (this is acceptable with the taut mooring system) we can use the approach of [26] and [19]. The plant dynamics are represented by the state-space system

$$\begin{aligned} \dot{\mathbf{x}}^{+} = \begin{bmatrix} \dot{\mathbf{x}} \\ \hline \ddot{\mathbf{x}} \\ \dot{\mathbf{p}}_r \end{bmatrix} &= \mathbf{A}\mathbf{x}^{+} + \mathbf{B}(\mathbf{F}_e + \mathbf{u}) \\ \mathbf{y} &= \mathbf{C}\mathbf{x}^{+} \end{aligned} \tag{6}$$

where $\mathbf{u}$ is the 6-DOF control force vector and the state vector is given by $[\mathbf{x} \;\; \dot{\mathbf{x}}]^T$. The state vector is augmented with the auxiliary states $\mathbf{p}_r$ relating to a 4^{th} order State-Space approximation $\mathbf{G}_r$ of the radiation impulse response functions described by

$$\begin{aligned} \dot{\mathbf{p}}_r &= \mathbf{A}_r\mathbf{p}_r + \mathbf{B}_r\dot{\mathbf{x}} \\ \int_0^t \mathbf{K}_r(t-\tau)\dot{\mathbf{x}}(\tau)d\tau &\approx \mathbf{C}_r\mathbf{p}_r + \mathbf{D}_r\dot{\mathbf{x}} \end{aligned} \tag{7}$$

where the matrices $\{\mathbf{A}_r, \mathbf{B}_r, \mathbf{C}_r, \mathbf{D}_r\}$ describing $\mathbf{G}_r$ are computed in the BEMIO code supplied with WEC-Sim [21]. Including all 36 modes in the state-space model results in 144 states. Figure 6 shows the BEM and approximated radiation impulse responses for the surge and heave modes showing the accuracy of the fitting process.

The augmented plant and output matrices are obtained from linearising the WEC system about its nominal resting position. These are given by equations 8-10 where $\mathbf{A}_\infty$ is obtained from the BEM solution, $\mathbf{K}_0$ is the linearised stiffness matrix (see [26]) and $\mathbf{B}_v$ is a linear viscous damping matrix empirically tuned to experimental data [22]. The state-space model order can be reduced by obtaining a balanced state-space realization and eliminating states with negligible contribution to the system response. Using this approach the total number of states can be reduced to 44, resulting in a model suitable for control system design.

Figure 7 shows the surge, heave and pitch float velocities under controlled conditions. Results are shown for three irregular sea states with the same peak period and increasing significant wave heights.

The reduced order linearised model shows good agreement, with accuracy reducing with increased wave height. This is to be expected as the model is linearised about its resting position and accuracy will degrade as the PTO tether angles change for large motions.

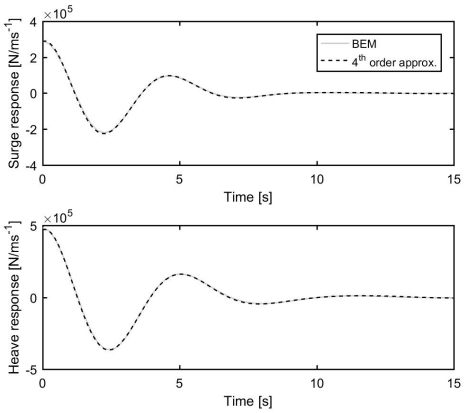

Fig. 6. Surge and heave radiation impulse responses from BEM solver and 4^{th} order aspproximation

$$\mathbf{A} = \left[\begin{array}{cc|c} \mathbf{0}^{6\times6} & \mathbf{I}^{6\times6} & \mathbf{0}^{6\times144} \\ -(\mathbf{M}+\mathbf{A}_\infty)^{-1}\mathbf{K}_0 & -(\mathbf{M}+\mathbf{A}_\infty)^{-1}(\mathbf{B}_v+\mathbf{D}_r) & -(\mathbf{M}+\mathbf{A}_\infty)^{-1}\mathbf{C}_r \\ \hline \mathbf{0}^{144\times6} & \mathbf{B}_r & \mathbf{A}_r \end{array}\right] \tag{8}$$

$$\mathbf{B} = \left[\begin{array}{c} \mathbf{0}^{6\times6} \\ (\mathbf{M}+\mathbf{A}_\infty)^{-1} \\ \hline \mathbf{0}^{144\times6} \end{array}\right] \tag{9}$$

$$\mathbf{C} = \left[\begin{array}{cc|c} \mathbf{0}^{6\times6} & \mathbf{I}^{6\times6} & \mathbf{0}^{6\times144} \end{array}\right] \tag{10}$$

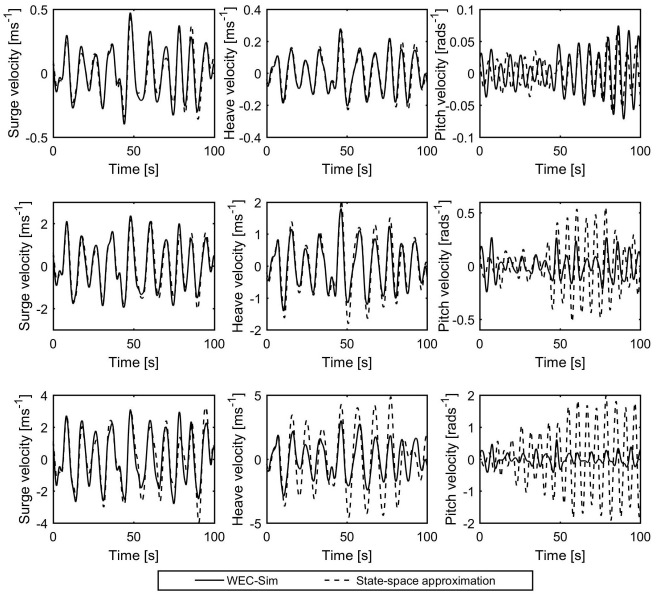

Fig. 7. Surge, heave and pitch float velocities under controlled conditions. Results shown for three sea states with $T_e = 10$s and $H_s = 1$m (TOP), $H_s = 3$m (MIDDLE), $H_s = 6$m (BOTTOM)

V. Active control methodology

As mentioned in section I, a practical WEC control strategy must be be robust to modelling errors and other uncertainty, but also must be simple to implement. Here we adopt the AVT strategy proposed in [18]. A velocity reference trajectory is evolved based upon the wave excitation force and

knowledge of the plant dynamics and constraints. If the PTO can be controlled so the float velocity tracks the reference then good power capture should be achieved. The overall control strategy is illustrated in Figure 8.

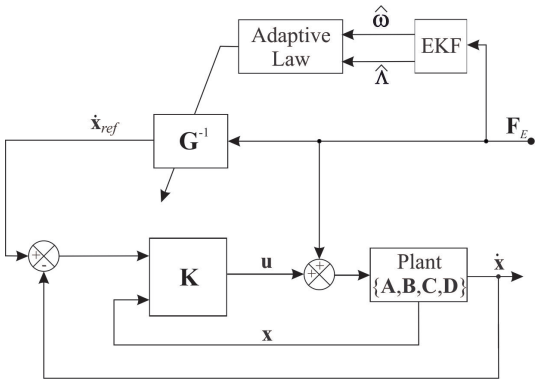

Fig. 8. Illustration of AVT control strategy with LQR velocity tracking (adapted from [18])

The vector of Cartesian velocity reference signals is given by

$$\dot{\mathbf{x}}_{ref}(t) = \mathbf{G}^{-1}(t)\mathbf{F}_e(t) = 0.5(|\mathbf{G}_r(\hat{\omega})| + \mathbf{B}_v)^{-1}\mathbf{F}_e(t) \tag{11}$$

where $|\mathbf{G}_r(\hat{\omega})|^{-1} \in R^{6\times 6}$ is the inverse of a time varying matrix of the instantaneous amplitudes of the 4^{th} order state space radiation damping model at the current estimated dominant excitation frequency $\hat{\omega}$. $\mathbf{F}_e(t)$ is assumed to be a narrow band harmonic process of the form [18]

$$\mathbf{F}_e(t) = \mathbf{\Lambda}\cos(\boldsymbol{\omega} t + \boldsymbol{\phi}) \tag{12}$$

It is necessary to estimate the dominant amplitude $\hat{\Lambda}$ and frequency $\hat{\omega}$ of the excitation force for each DOF. This is achieved using an extended Kalman filter (EKF) as described in section VI. Linear position constraints are required to avoid impacts between the float and reactor. Position constraints are readily incorporated as a velocity constraint under the narrow band assumption and the velocity reference gain has an upper bound given by $\bar{\mathbf{G}}^{-1} = \hat{\boldsymbol{\omega}}.\bar{\mathbf{x}}./\hat{\mathbf{\Lambda}}$ where $\{.\}$ denotes elementwise multiplication or division and $\{^-\}$ is the maximum permissible value of a quantity. Thus a real-time variable gain on the velocity reference may be expressed as

$$\mathbf{G}^{-1}(t) = \left\{ \begin{array}{ccc} 0.5(|\mathbf{G}_r| + \mathbf{B}_v)^{-1} : \bar{\mathbf{G}}^{-1} \geq 0.5(|\mathbf{G}_r| + \mathbf{B}_v)^{-1} \\ \\ \bar{\mathbf{G}}^{-1} \qquad : \qquad \text{otherwise} \end{array} \right\} \tag{13}$$

In this study the waves are unidirectional in the x-direction, so only surge and heave motion need to be controlled to prescribed trajectories.

Tracking of the velocity reference is achieved using a Linear Quadratic Regulator (LQR) state feedback controller under the assumption all states may be measured or accurately estimated. $\mathbf{K}$ is obtained from LQR optimisation to minimise the cost function

$$J(u) = \int_0^\infty \left(\mathbf{x}_e^T \mathbf{Q} \mathbf{x}_e + \mathbf{u}^T \mathbf{R} \mathbf{u}\right) dt \tag{14}$$

where $\mathbf{x}_e$ is the error state trajectory given by

$$\mathbf{x}_e = \left[\begin{array}{c} \mathbf{0}^{6\times 1} \\ \dot{\mathbf{x}}_{ref} \end{array} \right] - \left[\begin{array}{c} \mathbf{x} \\ \dot{\mathbf{x}} \end{array} \right] \tag{15}$$

The resulting state feedback gain is

$$\mathbf{K} = \mathbf{R}^{-1}\mathbf{B}^T\mathbf{S} \tag{16}$$

where $\mathbf{S}$ is the solution to the algebraic Riccati equation

$$\mathbf{A}^T\mathbf{S} + \mathbf{S}\mathbf{A} - \mathbf{S}\mathbf{B}\mathbf{R}^{-1}\mathbf{B}^T\mathbf{S} + \mathbf{Q} = 0 \tag{17}$$

and the weighting matrices are designed to balance control effort against tracking performance. Similar to [27], for $\mathbf{Q}$ we choose

$$\mathbf{Q} = \mathbf{C}^T\bar{\mathbf{Q}}\mathbf{C} \tag{18}$$

where $\bar{\mathbf{Q}} \in R^{6\times 6}$ is the auxiliary output error weighting matrix given by

$$\bar{\mathbf{Q}} = \frac{\bar{T}}{\bar{v}^2}\begin{bmatrix} |diag([\mathbf{e}_{si}])| & \mathbf{0}^{3\times 3} \\ \mathbf{0}^{3\times 3} & r.|diag(\mathbf{F}_i \times \mathbf{e}_{si})| \end{bmatrix} \tag{19}$$

where T and v are the PTO tether tension and velocity respectively, and r is the radius of the float. With reference to Figure 9, $\mathbf{F}_i$ is the float connection point coordinate vector relative to the float centre of gravity and $\mathbf{e}_{si}$ is the unit vector along the direction of the i^{th} PTO tether in the nominal WEC position. As the system has $x-y$ symmetry it does not matter which tether is used.

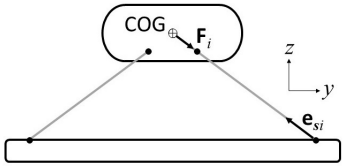

Fig. 9. Illustration of WEC kinematics

The control effort weighting is chosen as

$$\mathbf{R} = \frac{1}{\bar{T}}diag\left[\rho_1 \ \rho_2 \ ... \ \rho_6\right] \tag{20}$$

with ρ_i chosen appropriately to weight control effort in each DOF and achieve a compromise between good tracking performance, control effort and stability.

The control law in Cartesian coordinates is given as

$$\mathbf{u} = -\mathbf{K}\mathbf{x}_e \tag{21}$$

Distribution of $\mathbf{u}(t)$ to the four PTOs is achieved according to

$$\mathbf{u}_{PTO} = \mathbf{J}_0^T\mathbf{u} \tag{22}$$

where $\mathbf{J}_0^{-1}$ is the inverse kinematic Jacobian matrix given by [28]

$$\mathbf{J}_0^{-1} = \begin{bmatrix} \mathbf{e}_{s1}^T & (\mathbf{F}_1 \times \mathbf{e}_{s1})^T \\ \vdots & \vdots \\ \mathbf{e}_{s4}^T & (\mathbf{F}_4 \times \mathbf{e}_{s4})^T \end{bmatrix} \tag{23}$$

VI. Estimation of wave excitation force

The wave excitation or disturbance force is not measurable, but is required for the proposed control strategy. In order to estimate the disturbance force it is required to know the dynamics of the float body and all other forces acting upon it, as well as estimates or measurements of the float motion. Float motion and all forces other than the excitation force are readily measured or estimated as previously described. It this then possible to implement a dynamic observer to estimate the wave excitation force. Here we use a combination of Kalman filter approaches. First, we use the method described in [29], to estimate the excitation force. Then this is combined with the extended Kalman filter described in [30] to estimate the instantaneous amplitude and frequency of the estimated excitation force for use in the real-time controller. As we are able to measure the tether forces directly using load cells, we can directly measure the combination of control force and passive spring force.

The state vector $\mathbf{x}^+$ is further augmented with the unknown disturbance force $\mathbf{F}_e$ and its time-varying cyclical amplitude and frequency vectors $\mathbf{\Psi} = [\Lambda \ \Lambda^* \ \omega]$ for each relevant degree-of-freedom. The amplitude of the excitation force estimate is obtained as $\|\hat{\mathbf{F}}_e\| = \sqrt{\Lambda^2 + \Lambda^{*2}}$. Maintaining the notation $\mathbf{x}^+$ for the further augmented state vector for convenience, the discretized system dynamics are now described by

$$\mathbf{x}^+_{k+1} = \begin{bmatrix} \mathbf{x}^+ \\ \mathbf{F}_e \\ \mathbf{\Psi}_1 \\ \vdots \\ \mathbf{\Psi}_n \end{bmatrix}_{k+1} = \mathbf{A}^+\mathbf{x}^+_k + \mathbf{B}^+ \left(\mathbf{F}_e - \mathbf{T}\right)_k + \boldsymbol{\epsilon}_k$$
$$\mathbf{y} = \mathbf{C}^+\mathbf{x}^+_k + \boldsymbol{\mu}_k \tag{24}$$

where $\boldsymbol{\epsilon}$ describes the random walk process for excitation force estimation and unmodelled dynamics, and $\boldsymbol{\mu}$ describes measurement noise. $\mathbf{T}$ is the Cartesian vector of PTO forces, derived from direct measurement of the combined control and spring forces as PTO tether tensions $\mathbf{T}_{PTO}$ according to

$$\mathbf{T} = \mathbf{J}_0^{-T}\mathbf{T}_{PTO} \tag{25}$$

where $\mathbf{J}_0^{-T}$ is the transpose of the inverse kinematic Jacobian matrix. The system matrices are defined as follows:

$$\mathbf{A}^+ = \begin{bmatrix} \mathbf{A} & \mathbf{B} & \mathbf{0} & \mathbf{0} & \mathbf{0} \\ \mathbf{0} & \mathbf{I} & \mathbf{0} & \mathbf{0} & \mathbf{0} \\ \mathbf{0} & \mathbf{0} & \mathbf{A}^c_1 & \mathbf{0} & \mathbf{0} \\ \mathbf{0} & \mathbf{0} & \mathbf{0} & \ddots & \mathbf{0} \\ \mathbf{0} & \mathbf{0} & \mathbf{0} & \mathbf{0} & \mathbf{A}^c_n \end{bmatrix} \quad \mathbf{B}^+ = \begin{bmatrix} \mathbf{B} \\ \mathbf{0} \\ \mathbf{0} \\ \vdots \\ \mathbf{0} \end{bmatrix}$$
$$\mathbf{C}^+ = \begin{bmatrix} \mathbf{C} & \mathbf{D} & \mathbf{0} & \mathbf{0} & \mathbf{0} & \mathbf{0} & \mathbf{0} & \mathbf{0} & \mathbf{0} \\ 0 & 0 & (1 & 0 & 0) & 0 & 0 & 0 & 0 \\ 0 & 0 & 0 & 0 & 0 & \ddots & 0 & 0 & 0 \\ 0 & 0 & 0 & 0 & 0 & 0 & (1 & 0 & 0) \end{bmatrix} \tag{26}$$

where, for the i^{th} degree of freedom,

$$\mathbf{A}^c_i = \begin{bmatrix} \cos\omega_i\Delta t & \sin\omega_i\Delta t & 0 \\ -\sin\omega_i\Delta t & \cos\omega_i\Delta t & 0 \\ 0 & 0 & 1 \end{bmatrix} \tag{27}$$

where Δt is the sampling interval and $\{\mathbf{A}, \mathbf{B}, \mathbf{C}\}$ are first-order hold discretised versions of equations 8 to 10 but with the stiffness matrix $\mathbf{K}_0$ set to $\mathbf{0}^{6\times1}$ as this force is measured, and $\mathbf{0}$ are zero matrices of appropriate dimensions.

The prediction step estimates the next state $\hat{\mathbf{x}}^+_{k|k-1}$ and covariance $\mathbf{P}^+_{k|k-1}$ matrices as:

$$\begin{aligned}\hat{\mathbf{x}}^{+}_{k|k-1} &= \mathbf{A}^{+}_{k-1}\hat{\mathbf{x}}^{+}_{k-1|k-1} - \mathbf{B}^{+}\mathbf{T}_{k-1|k-1} \\ \mathbf{P}^{+}_{k|k-1} &= \mathbf{J}^{+}_{k-1}\mathbf{P}^{+}_{k-1|k-1}\mathbf{J}^{+T}_{k-1} + \mathbf{Q}^{+}_{k-1}\end{aligned} \tag{28}$$

where $\mathbf{Q}^{+}$ is the process noise covariance matrix, assumed to represent a zero mean Gaussian process. The update step is defined by:

$$\begin{aligned}\mathbf{S}^{+}_{k} &= \mathbf{C}^{+}_{k}\mathbf{P}^{+}_{k}\mathbf{C}^{+T}_{k} + \mathbf{R}^{+}_{k} \\ \mathbf{K}^{+}_{k} &= \mathbf{P}^{+}_{k}\mathbf{C}^{+T}_{k}\mathbf{S}^{+^{-1}}_{k} \\ \hat{\mathbf{x}}^{+}_{k|k} &= \hat{\mathbf{x}}^{+}_{k|k-1} + \mathbf{K}^{+}_{k}\left(\begin{bmatrix}\mathbf{y}_k & \hat{\mathbf{F}}_e\end{bmatrix}^{T} - \mathbf{C}^{+}_{k}\hat{\mathbf{x}}^{+}_{k|k-1}\right) \\ \mathbf{P}^{+}_{k|k} &= (I - \mathbf{K}^{+}_{k}\mathbf{C}^{+}_{k})\mathbf{P}^{+}_{k|k-1}\end{aligned} \tag{29}$$

where $\mathbf{S}^{+}$ is the innovation residual, $\mathbf{R}^{+}$ is the observation covariance associated with the observed value $\mathbf{y}$, and $\mathbf{K}$ is the Kalman gain. $\mathbf{J}^{+}$ is the Jacobian of $\mathbf{A}^{+}$ which is recalculated every time step as $\mathbf{A}^{c}$ is time-varying.

Figure 10 shows good estimation of the excitation force for surge and heave directions, and Figure 11 shows the amplitude and frequency estimation of an observed signal for the wave excitation force in surge and heave for irregular waves obtained from the Wec-Sim simulation. Good estimation of instantaneous amplitude and frequency is achieved.

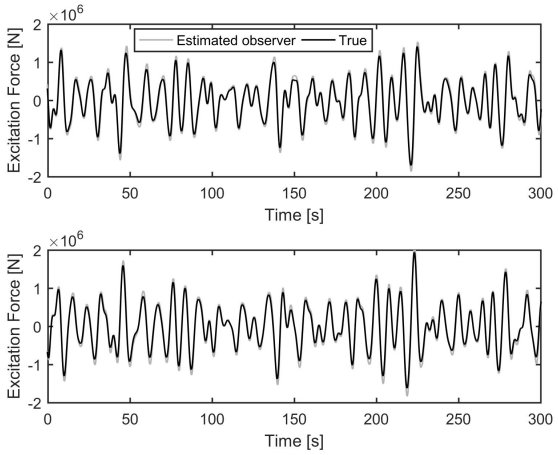

Fig. 10. Estimation of wave excitation force in surge and heave directions in irregular waves (Pierson-Moskowitz with $H_s = 3$m, $T_e = 10$s)

VII. Simulation results

All simulations were conducted using WEC-Sim V2.1 with Matlab2017b. A 4^{th} order Runge-Kutta solver was used with a sampling interval of 0.02s. All simulations were 700s in duration. For detailed insight into the actively controlled system performance, the irregular sea-state of Figure 4 was imposed upon the full nonlinear WEC-Sim model.

A. Velocity reference tracking

Figure 12 shows the surge and heave reference and measured float velocities. An achievable velocity reference signal has been generated and the active control strategy is clearly seen to provide good tracking.

Displacement limits from nominal of ± 5m in surge and ± 3m in heave were imposed. Figure 13 shows that the displacement limits are largely adhered to.

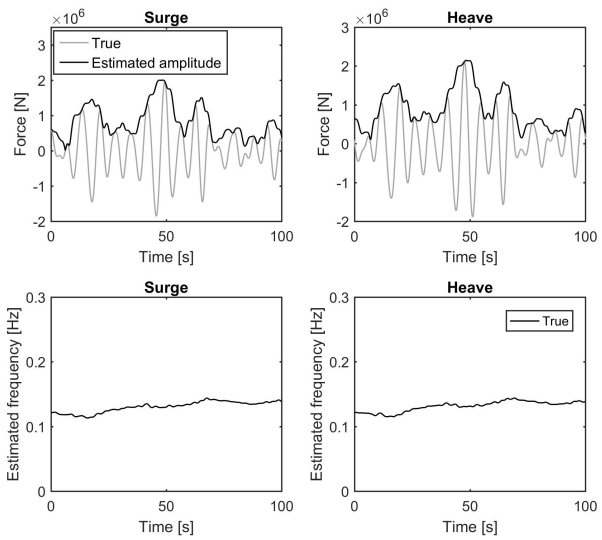

Fig. 11. EKF wave force amplitude and frequency estimation

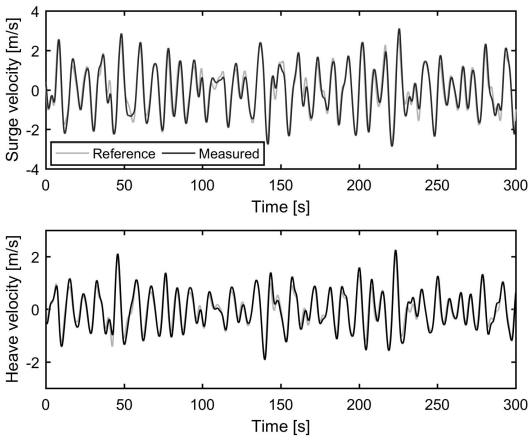

Fig. 12. Surge and heave reference and measured float velocities under controlled conditions (sea state $H_s = 3$m, $T_e = 10$s) for full WEC-Sim model

These limits are imposed in a soft manner, so a factor of safety can be applied if it is critical that they are not exceeded. Though it is not controlled, the pitch motion is included for completeness. Also shown are the motions under passive control for comparative purposes.

B. Load limiting

Figure 14 shows the % increase in peak PTO tether tension for the actively controlled system compared to the passively controlled benchmark for irregular sea states with different significant wave heights.

The peak tether tensions are larger for the actively controlled system as expected, being up to 60% higher than the passive system peak values. Figure 15 shows the applied PTO control forces and the resulting PTO tether tensions which are the combination of the control force, pre-tension and spring force. If the control force is not constrained the tether tensions are seen to become positive occasionally. In larger seas this effect would be more prevalent. In reality this is not possible and the PTO tethers would become slack, causing issues for controllability and potentially resulting in large snatching loads being transmitted which would reduce the lifetime of the WEC and PTO. Therefore it is necessary to introduce a dynamic saturation constraint on $\mathbf{u}$, such that $\Delta\mathbf{u} \leq \mathbf{T}$, where $\Delta\mathbf{u}$ is the

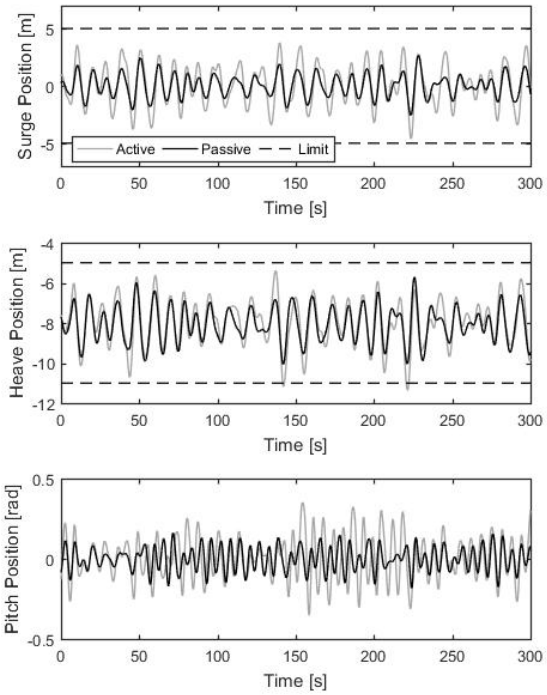

Fig. 13. Surge, heave and pitch float positions under controlled conditions (sea state $H_s = 3$m, $T_e = 10$s) for full WEC-Sim model

change in control force from the current time step and **T** is the vector of measured tether tensions. Figure 15 also shows the control forces and line tensions using this constraint, it can be seen that the tethers remain taught.

C. Power capture

Figure 16 shows the instantaneous and mean generated power for the passive and actively controlled systems. It should be noted that negative power indicates power flow from the WEC to the grid. Increased power is clearly seen for the actively controlled system, though it would also require more smoothing than the passively controlled output. The reactive power component is clearly seen as positive power when the controller commands a motoring action from the PTOs. This is not always possible or desirable due to the increased cost and complexity of components. Two-quadrant operation may be favourable in many situations, and operates as a restriction of uni-directional power flow i.e. the generator can only generate in both directions, motoring is not permitted. This restriction may be readily incorporated to the active control strategy. This will impact on system performance, but the benefits come in the form of reduced cost and complexity of the components required to achieve the PTO power generation. Alternatively, it has been shown in [31] that the reactive power requirement can be provided in the Power Electronic Converter using supercapacitor short term energy storage.

Figure 17 shows the percentage increase in mean power generation achieved by the actively controlled system over 700s of simulation with the full nonlinear WEC-Sim model. The results are shown for irregular PM spectra with $H_s = 0.5 - 6.5$m and $T_e = 6 - 16$s, with and without the control

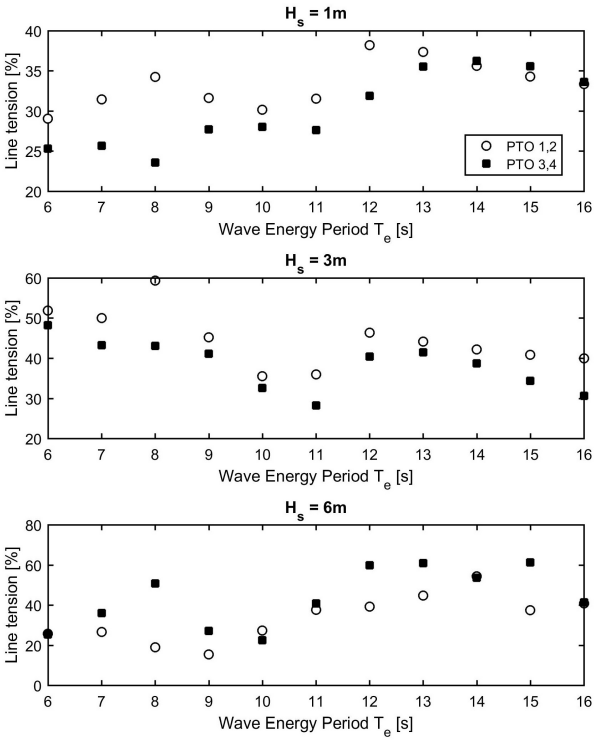

Fig. 14. % increase in peak PTO tether tension for active compared to passive control for full WEC-Sim model. Results shown for irregular sea states with a range of T_e and $H_s = 1$m (TOP), $H_s = 3$m (MIDDLE), $H_s = 6$m (BOTTOM)

force constraint (in total 143 irregular wave cases). Power gains of up to 80% are observed across a wide range of irregular sea states compared to the passive system. A slight reduction in power is seen with the control force constraint active.

It is important to note that all performance gains reported here are relative to the optimally tuned passive system. This means that the passive system damping coefficient was individually tailored to a given sea state. The power capture of the passive system is very sensitive to this damping coefficient, and large power reductions would be seen for a detuned system. The passive system damping coefficient would need to be adjusted in service based upon the peak period of the sea state estimated from measurement. This process is subject to errors, particularly for sea states with multiple peaks. Therefore the performance benefits of the actively controlled system would be expected to be greater in a deployed system, as it is not reliant on such measurements and the inherent uncertainty associated with them.

VIII. Conclusions

The aim of this study was to develop an active control strategy for the multi-DOF submerged point absorber WaveSub WEC and related devices. Many previous studies assume the WEC to be a simplified 1-DOF system, and the controller is built around a model exactly matching this. In reality there will be model mismatch and this will impact on the performance and robustness of the controller. Additionally, many studies assume perfect knowledge of the wave excitation force — a necessary input to many control strategies. Again, this is not feasible in reality. One of the key requirements of this study was that the controller should be deployable — i.e. it does not rely on inputs which cannot be measured or estimated in a real system. To this end we have designed an approximate optimal velocity controller, which generates the optimal velocity trajectory for the prime mover using the estimated wave excitation force. The excitation force is estimated from measurable quantities using a Kalman filter approach. A linear quadratic regulator is used to perform velocity tracking, and a robust tuning method is developed to balance performance against control effort and stability. The regulator is built using a linearised model of the WEC, but the controller is tested

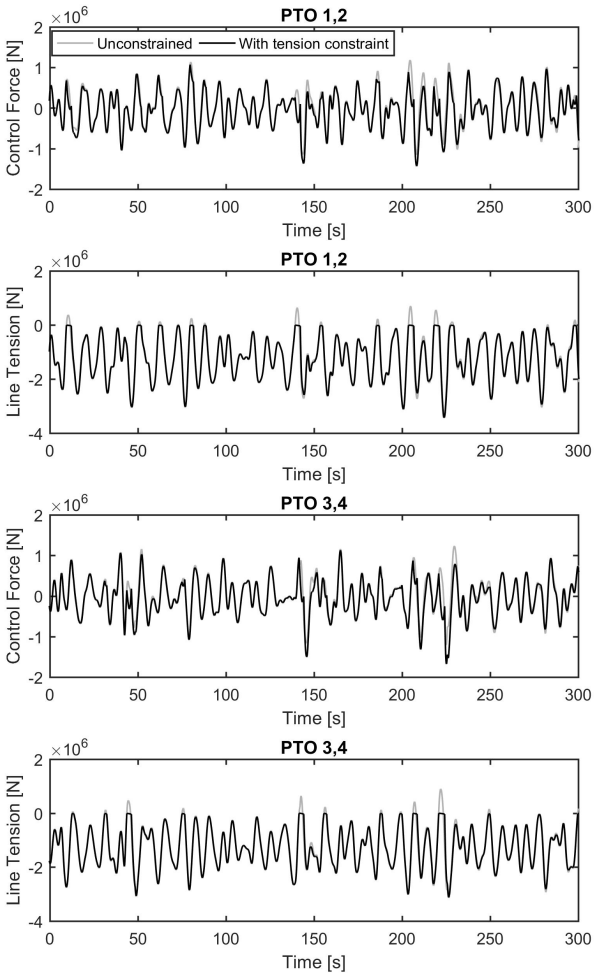

Fig. 15. Control forces and tether tensions under controlled conditions (sea state $H_s = 3$m, $T_e = 10$s) for full WEC-Sim model

with a validated nonlinear multi-body simulation with full kinematic constraints. As such, model mismatch between the controller and the controlled system is present. A further constraint was to impose a dynamic force control limit to avoid snatching loads in PTO tethers, which would result in a reduced device lifetime and possibly catastrophic damage. Thus the simulations conducted are closer to reality than many previous studies, and the developed controller can be considered deployable in real time. These are the main contributions of the work.

The performance of the active control system was compared against an optimally tuned passively damped system — a commonly used benchmark. For this study the stiffness and damping values of the PTO were tuned to each irregular sea state (a total of 143 cases covering a full range of realistic operating conditions), thus the comparison is not against a de-tuned system and the performance gains are not exaggerated. Excellent performance was observed for the actively controlled system. Mean power increases of up to 80% were seen compared to the optimal passive system, and the control strategy was shown to be robust to parameter uncertainty. Therefore this approach shows promise to provide a substantial increase in power capture for a minimal additional device cost and therefore a significant improvement in cost of energy would likely result. Of course, this study is limited to simulation only. Experimental validation of the controller is a subject of further work.

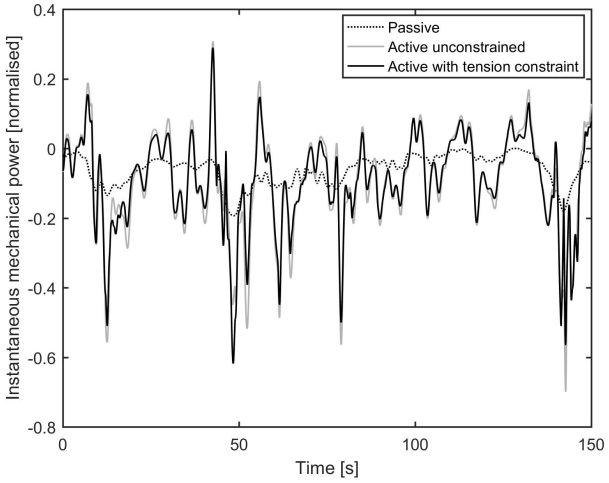

Fig. 16. Instantaneous power under controlled conditions (sea state $H_s = 3$m, $T_e = 10$s) for full WEC-Sim model

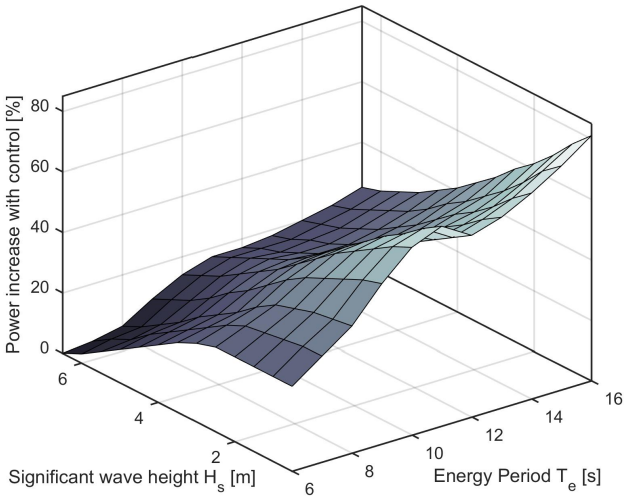

Fig. 17. Power matrix showing power percentage increase compared to optimal passive benchmark system for a range of irregular seas with peak period T_e and significant wave height H_s

REFERENCES

[1] Carbon Trust technical report. UK Wave Energy Resource. 2012.

[2] R C T Rainey. Key features of wave energy. *Philosophical transactions. Series A, Mathematical, physical, and engineering sciences*, 370:425–38, 01 2012.

[3] J. Falnes. A review of wave-energy extraction. *Marine Structures*, 20:185–201, 2007.

[4] A. Babarit, G. Duclos, and A.H. Clément. Comparison of latching control strategies for a heaving wave energy device in random sea. *Applied Ocean Research*, 26(5):227–238, 2005.

[5] A.F.O. Falcão. Modelling and control of oscillating-body wave energy converters with hydraulic power take-off and gas accumulator. *Ocean Engineering*, 24:2021–2032, 2007.

[6] A.F.O. Falcão. Phase control through load control of oscillating-body wave energy converters with hydraulic PTO system. *Ocean Engineering*, 35:358–366, 2008.

[7] J.A.M. Cretel, G. Lightbody, G.P. Thomas, and A.W. Lewis. Maximisation of energy capture by a wave-energy point absorber using model predictive control. In *Proceedings of the 18th IFAC World Congress*, volume 44, pages 3714 – 3721, Milan, Italy, 2011.

[8] J. Hals, J. Falnes, and T. Moan. Constrained optimal control of a heaving buoy wave-energy converter. *Journal of Offshore Mechanics and Arctic Engineering*, 133(1):011401–011401, 2010.

[9] G. Bacelli, J.V. Ringwood, and J-C. Gilloteaux. A control system for a self-reacting point absorber wave energy converter subject to constraints. In *Proceedings of the 18th IFAC World Congress*, volume 44, pages 11387 – 11392, Milian, Italy, 2011.

[10] M. Richter, M. E. Magana, O. Sawodny, and T. K. A. Brekken. Nonlinear model predictive control of a point absorber wave energy converter. *IEEE Transactions on Sustainable Energy*, 4(1):118–126, 2013.

[11] R. Genest and J.V. Ringwood. A critical comparison of model-predictive and pseudospectral control for wave energy devices. *Journal of Ocean Engineering and Marine Energy*, 2(4):485–499, Nov 2016.

[12] H-N. Nguyen and P. Tona. An efficiency-aware continuous adaptive proportional-integral velocity-feedback control for wave energy converters. *Renewable Energy*, 146:1596 – 1608, 2020.

[13] O. Abdelkhalik, S. Zou, R. D. Robinett, G. Bacelli, D. G. Wilson, R. Coe, and U. Korde. Multiresonant feedback control of a three-degree-of-freedom wave energy converter. *IEEE Transactions on Sustainable Energy*, 8(4):1518–1527, Oct 2017.

[14] O. Abdelkhalik, S. Zou, G. Bacelli, D. G. Wilson, and R. Coe. Control of three degrees-of-freedom wave energy converters using pseudo-spectral methods. *ASME. J. Dyn. Sys., Meas., Control*, 140(7), 2018.

[15] D.V. Evans, D.C. Jeffrey, S.H. Salter, and J.R.M. Taylor. Submerged cylinder wave energy device: theory and experiment. *Applied Ocean Research*, 1(1):3 – 12, 1979.

[16] S. Crowley, R. Porter, and D. V. Evans. A submerged cylinder wave energy converter. *Journal of Fluid Mechanics*, 716:566–596, 2013.

[17] S. S. Ngu, D. G. Dorrell, and E. Acha. Control of a Bristol cylinder for wave energy generation. In *The 2010 International Power Electronics Conference - ECCE ASIA -*, pages 3196–3203, June 2010.

[18] F. Fusco and J. V. Ringwood. A simple and effective real-time controller for wave energy converters. *IEEE Transactions on Sustainable Energy*, 4(1):21–30, 2013.

[19] N. Sergiienko, B. Cazzolato, P. Hardy, B. Ding, and M. Arjomandi. Internal-model-based velocity tracking control of a submerged three-tether wave energy converter. In *Proceedings of the Twelfth European Wave and Tidal Energy Conference*, Cork, Ireland, 2017.

[20] A.J. Hillis, J. Roesner, N.P. Sell, D.R.S. Chandel, and A.R. Plummer. Investigation of the benefits of adaptive control applied to the nonlinear CCell wave energy converter. In *Proceedings of the Twelfth European Wave and Tidal Energy Conference*, Cork, Ireland, 2017.

[21] Y. Yu, M. Lawson, K. Ruehl, and C. Michelen. Development and demonstration of the wec-sim wave energy converter simulation tool. In *Proceedings of the 2nd Marine Energy Technology Symposium, Seattle, WA*, 2014.

[22] E. Faraggiana, C. Whitlam, J. Chapman, A. Hillis, J. Roesner, M. Hann, D. Greaves, Y.-H. Yu, K. Ruehl, I. Masters, G. Foster, and G. Stockman. Computational modelling and experimental tank testing of the multi float wavesub under regular wave forcing. *Renewable Energy*, 152:892 – 909, 2020.

[23] W. E. Cummins. The Impulse Response Function and Ship Motions. *Schiffstechnik*, 9:101–109, 1962.

[24] A. Babarit and G. Delhommeau. Theoretical and numerical aspects of the open source BEM solver NEMOH. In *Proceedings of the 11th European Wave and Tidal Energy Conference*, Nantes, France, 2015.

[25] C.J. Cargo, A.J. Hillis, and A.R. Plummer. Strategies for active tuning of wave energy converter hydraulic power take-off mechanisms. *Renewable Energy*, 94:32 – 47, 2016.

[26] J.T. Scruggs, S.M. Lattanzio, A.A. Taflanidis, and I.L. Cassidy. Optimal causal control of a wave energy converter in a random sea. *Applied Ocean Research*, 42:1 – 15, 2013.

[27] G. Vissio, D. Valério, G. Bracco, P. Beirão, N. Pozzi, and G. Mattiazzo. Iswec linear quadratic regulator oscillating control. *Renewable Energy*, 103:372 – 382, 2017.

[28] N.Y. Sergiienko, A. Rafiee, B.S. Cazzolato, B. Ding, and M. Arjomandi. Feasibility study of the three-tether axisymmetric wave energy converter. *Ocean Engineering*, 150:221 – 233, 2018.

[29] H-N. Nguyen and P. Tona. Wave excitation force estimation for wave energy converters of the point-absorber type. *IEEE Transactions on Control Systems Technology*, 26(6):2173–2181, Nov 2018.

[30] F. Fusco and J. V. Ringwood. Short-term wave forecasting for real-time control of wave energy converters. *IEEE Transactions on Sustainable Energy*, 1(2):99–106, July 2010.

[31] A.J. Hillis, A.R. Plummer, X. Zeng, and J. Chapman. Simulation of a power electronic conversion system with short-term energy storage for actively controlled wave energy converters. In *Proceedings of the 6th Offshore Energy and Storage Summit*, Brest, France, 2019.